Journal of Chromatography A 1653 (2021) 462398

Contents lists available at ScienceDirect

Journal of Chromatography A

journal homepage: www.elsevier.com/locate/chroma

Evaluation of guanidine-based multimodal anion exchangers for protein selectivity and orthogonality

Sushmita Koley[a], Scott H. Altern[a], Mayank Vats[a], Xuan Han[a], Dongyoun Jang[a], Mark A. Snyder[b], Chris Belisle[b], Steven M. Cramer[a,*]

[a] Department of Chemical and Biological Engineering and Center for Biotechnology and Interdisciplinary Studies, Rensselaer Polytechnic Institute, Troy, NY 12180, United States
[b] Bio-Rad Laboratories, Hercules, CA 94547 United States

ARTICLE INFO

Article history:
Received 5 April 2021
Revised 2 July 2021
Accepted 3 July 2021
Available online 9 July 2021

Key words:
Multimodal chromatography
Protein separations
Guanidine based ligands
Orthogonality

ABSTRACT

In this paper, we examined the chromatographic behavior of a new class of guanidine-based multimodal anion exchange resins. The selectivities and protein recoveries on these resins were first evaluated using linear gradient chromatography with a model acidic protein library at pH 5, 6 and 7. While a single-guanidine based resin exhibited significant recovery issues at high ligand density, a bis-guanidine based resin showed high recoveries of all but two of the proteins evaluated in the study. In addition, the bis-guanidine resin showed a more pH dependent selectivity pattern as compared to the low density single-guanidine resin. The salt elution range for the low density single-guanidine and bis-guanidine resins was also observed to vary from 0.250 to 0.621 M and 0.162 to 0.828 M NaCl, respectively. A QSAR model was then developed to predict the elution behavior of these proteins on the guanidine prototypes at multiple pH with overall training and test scores of 0.88 and 0.85, respectively. In addition, molecular dynamics simulations were performed with these ligands immobilized on a self-assembled monolayer (SAM) to characterize their conformational preferences and to gain insight into the molecular basis of their chromatographic behavior. Finally, a recently developed framework was employed to evaluate the separability of the bis-guanidine resin as well as its orthogonality to the multimodal cation exchanger, Nuvia cPrime. This evaluation was carried out using a second model protein library which included both acidic and basic proteins. The results of this analysis indicated that the bis-guanidine prototype exhibited both higher pair separability (0.73) and pair enhancement (0.42) as compared to the less hydrophobic commercial Nuvia aPrime 4A with pair separability and enhancement factors of 0.57 and 0.22, respectively. The enhanced selectivity and orthogonality of this new multimodal anion exchange ligand may offer potential opportunities for bioprocessing applications.

1. Introduction

Multimodal (MM) ion exchange chromatography has been demonstrated to have enhanced selectivity as compared to traditional single mode interaction resins due to the multiple interactions (electrostatic, hydrophobic, aromatic and/or hydrogen bonding) that these ligands can have with a given solute [1–4]. This improved selectivity in concert with higher salt tolerance has made these materials particularly useful for clearing process and/or product-related impurities [5] and may enable the elimination of affinity capture [6–8] steps. Multimodal cation exchangers (MMC) have been extensively studied both with respect to their fundamental interactions [9–13] and bioprocessing applications [14–19]. Woo et al. examined the impact of the spatial organization of hydrophobic and charged moieties on MMC ligands on protein retention behavior [9,10]. In that work it was observed that the hydrophobic moieties and their solvent exposure played an important role in the selectivities that could be achieved [10]. Importantly, there have been several reports evaluating MMC resins for their ability to capture monoclonal antibodies directly from cell culture supernatant as an alternative to Protein A [18,20]. Further, MMC materials have been shown to be effective for the clearance of product and process impurities in post protein A monoclonal antibody polishing operations [21,22].

Multimodal anion exchangers (MMA) have also been studied in the literature [2]. The use of MMA resins in the flow-through mode for the removal of product-related impurities such as aggregates, and antibody fragments has been widely reported [23–25].

* Corresponding author.
E-mail address: crames@rpi.edu (S.M. Cramer).

https://doi.org/10.1016/j.chroma.2021.462398
0021-9673/

Johansson et al. demonstrated that while aromatic multimodal anion exchangers exhibited protein recovery issues, this was not observed for non-aromatic based ligands which contained primary or secondary amines [26]. Robinson et al. evaluated the selectivity trends of a model protein set using three series of structural variants of the commercial adsorbent, Nuvia aPrime 4A [27]. While subtle differences in selectivity were achieved, the effects were less pronounced than those observed with the MMC ligand libraries reported in the literature [9,10]. In the current study, we develop a new class of MMA resins that have more salt tolerance than Capto Adhere and the Nuvia aPrime based resins, as well as unique selectivities for the less retained proteins [27]. In contrast to previous work, these new prototypic ligands have the charge moiety in the form of either a single or bis guanidine-group. This is contrast to the resins discussed above as well as other MMA adsorbents such as MEP HyperCel™, PPA HyperCel™ and HEA HyperCel [28–31] which have their charged moiety based on either substituted-amine or pyridine-based chemistries.

There is significant interest in the development of integrated downstream bioprocesses [6] where the individual unit operations offer a degree of orthogonality with respect to impurity removal. This requires the identification of resin combinations that will enable the removal of impurities in an orthogonal manner [32]. We have recently developed a mathematical framework to quantify separability and orthogonality for resin sets using model protein libraries [33]. One of the results of that study was that resins that can probe a range of hydrophobic and electrostatic interactions can be useful in this context.

Shukla and Trout have studied the inhibition of protein aggregation using arginine [34,35] and shown that arginine interacted with the protein surfaces primarily through π-cation interactions of the guanidinium moiety. The ability of guanidine to interact with both negatively charged and aromatic residues on proteins motivated us to synthesize and evaluate the new class of guanidinium-based multimodal anion exchange resins described here.

In this paper, we examine the chromatographic behavior of a new class of guanidine-based multimodal anion exchange resins. The selectivities and protein recoveries on these resins is evaluated with a model acidic protein library at pH 5, 6 and 7. The results indicate that the bis-guanidine resin has high salt tolerance and recoveries as well as more pH dependent selectivity patterns. A QSAR model is then developed to predict the elution behavior of these proteins on the guanidine prototypes at multiple pH. Molecular dynamics simulations are then carried out to characterize ligand conformational preferences and to gain insights into the molecular basis of the chromatographic behavior. Finally, a recently developed framework is employed to evaluate the separability of the bis-guanidine resin as well as its orthogonality to the multimodal cation exchanger, Nuvia cPrime.

2. Materials and methods

2.1. Materials

The guanidine-based multimodal anion exchangers (MMA) prototypes with varying ligand densities and the commercial Nuvia aPrime 4A and Nuvia cPrime resins were provided by Bio-Rad Laboratories (Hercules, CA). Capto Adhere was purchased from Cytiva (Marlborough, MA). The proteins α-lactalbumin, α-chymotrypsinogen A, α-chymotrypsin, β-lactoglobulin A (BLA), β-lactoglobulin B (BLB), albumin (rabbit), bovine serum albumin (BSA), carbonic anhydrase, cellulase, conalbumin, concanavalin, human serum albumin (HSA), horse cytochrome C, lactoferrin, lectin, lysozyme, ovalbumin, ribonuclease B, transferrin, trypsin inhibitor and ubiquitin were obtained from Sigma Aldrich (St. Louis, Mo.). Human growth hormone (hGH) was generously supplied by Novo Nordisk (Bagsværd, Denmark) and mAb A was generously supplied by AstraZeneca (Cambridge, UK). Acetonitrile and HCl were purchased from Sigma Aldrich. 96-well 350μL sample collection plates, 96- well plate mats, Acquity UPLC Protein BEH C4 columns (300 angstrom, 1.7 µm, 2.1 mm x 100 mm), and Acquity UPLC Protein BEH VanGuard PreColumns (300 angstrom, 1.7 µm, 2.1 mm x 5 mm) were purchased from Waters Corporation (Milford, MA). HPLC grade trifluoroacetic acid (TFA) and glacial acetic acid were purchased from Thermo Fisher Scientific (Pittsburgh, PA).

2.2. Chromatography experiments

2.2.1. Retention/Selectivity

Chromatographic resins were initially washed with deionized water and a 50% (v/v) slurry was made. The resins were then packed in 5 × 50 mm glass columns and the adapter was adjusted to a final bed volume of ~ 1 mL. The asymmetry of the packed columns was determined by first moment analysis of an acetone pulse and only columns with values between 0.8 and 1.2 were used. Chromatography experiments were performed using an Äkta Explorer 100 (Amersham Biosciences, Uppsala, Sweden) controlled by Unicorn 5.31 software. Linear salt gradients were carried out 0 to 100% Buffer B over 40 column volumes (CV) at a flow rate of 1 CV / min and then held at 100% B for 10 CV. For the pH 6 and 7 experiments, buffer A was 10 mM sodium phosphate at the appropriate pH and buffer B was the same solution with 1.5 M NaCl. For pH 5, buffer A was 10 mM sodium acetate and buffer B was the same solution with 1.5 M NaCl. The acidic proteins evaluated in this section were loaded on the columns at 2 mg protein per ml adsorbent and the retention times were determined from the first moments of the elution peaks. The corresponding elution salt concentrations (mM) were then determined from the conductivity trace.

2.2.3. Separability and orthogonality evaluations

The procedure for obtaining the protein retention data and for determining the separability and enhancement factors are described elsewhere [33]. A 15 protein set that included both acidic and basic model proteins as well as mAb A with varying levels of hydrophobicity were grouped into three sets (mixtures) of five proteins based on their relative retention times in UP-RPLC gradients. Linear salt gradients were performed for each mixture, on the AKTA system, at pH 5.0, 6.0, and 7.0 from 0 to 1.5 M NaCl. For linear gradient experiments at pH 5.0, 20 mM sodium citrate buffer was used, while 20 mM sodium phosphate buffer was used for pH 6.0 and 7.0. Two strip solutions were used for each resin system—a non-denaturing strip of 100 mM Tris base, for MMC, and 100 mM citric acid, for MMA, both with added 1 M NaCl. A harsh strip of 0.5 M NaOH was used for both resin functionalities to regenerate the column after the non-denaturing strip step. Fractions of the flow-through, gradient, and non-denaturing strip were collected at a resolution of 1 CV for each chromatography run. Each fraction was then analyzed with RP-UPLC gradients to determine the relative absorbance of each protein present. A method of peak deconvolution, using the RP-UPLC absorbance values across fractions, was subsequently employed to extract the chromatogram of each protein included in the set. First moment analysis of the chromatographic data was then performed to construct a database of retention values for each protein on each resin studied—the bis-guanidine MMA prototype, Nuvia aPrime 4A, and Nuvia cPrime.

After this, the distance distribution method described in was used to calculate the pairwise distances (d_{ab}) between proteins—the difference in their retention values. These distances were used to generate weights based on rescaling the gradient according to the difference in retention between the most strongly and least

strongly retained proteins (Eq. (1)). Here, r_{low} represents the lower bound where all proteins are co-eluting, ⅛ of the rescaled gradient, while r_{high} represents the upper bound where all proteins are completely separated, ½ of the rescaled gradient. For every pair of proteins (a and b), the weights ($w_{a,b}$) were calculated to represent the degree of success in their separation. Separability factors (S) were calculated by taking an average value of the weights and represents the ability of a given resin or resin set to separate all protein pairs within the entire protein pool (Eq. (2)). Lastly, enhancement factors (E_m) were determined by calculating the fractional improvement of the separability factor when adding an additional resin to the resin set (Eq. (3)).

$$w_{a,b} = \begin{cases} 0 & d_{ab} < r_{low} \\ \frac{d_{ab} - r_{low}}{r_{high} - r_{low}} & r_{high} \geq d_{ab} \geq r_{low} \\ 1 & d_{ab} > r_{high} \end{cases} \quad (1)$$

$$S = \frac{1}{\binom{n}{2}} \sum_{a=1}^{n-1} \sum_{b=a+1}^{n} w_{ab} \quad (2)$$

$$E_m = \frac{S_m}{\max\left(S_{m-1} \forall (m-1) \in m\right)} \quad (3)$$

2.2.4. Descriptor calculations

Molecular descriptors were calculated both for proteins and ligands used in this study. Structures of proteins were acquired (Table-S1) through Protein Data Bank (PDB) and structures of ligands were prepared using Molecular Operating Environment (MOE) from Chemical Computing Group (Montreal, Canada). MOE was also used for calculating ligand descriptors and protein global descriptors. Other protein surface properties related descriptors were calculated using in-house scripts according to the procedure published previously [9]. In total, 233 protein descriptors and 343 ligand descriptors were generated for Quantitative Structure Relationship (QSAR) model development.

2.2.5. QSAR model development

Model development was implemented using python 3.7.1 on JupyterLab 2.1.5. Model was developed upon elution behaviors of 10 model proteins (Table-S1) associating with single guanidine ligand (Prototype 15) and bis-guanidine ligand (Prototype 6611 9–1) under pH 5, 6, 7. Proteins that did not elute during the gradient were excluded from the model development, resulting in 48 data points in total. Randomly selected 5 data points were used as external test set and rest 43 data points were used for model training. Standardization was applied for all the descriptors prior to feature selection. Recursive feature elimination based on descriptors weights in the model and variable influence on projection (VIP) score [27] were utilized for feature selection. Partial least square (PLS) with optimized number of principal components was applied for training the model. Average score of 10 times 5-fold cross validation and 50-round Y-scrambling were used for model validation.

2.2.6. Molecular dynamics simulations

Ligand immobilized SAM surfaces were prepared using a setup described previously by our group [36–38]. Single leaflet SAM strands were prepared comprising of 10 carbon atoms with one sulfur and carbon atom at the base and capped with a protype ligand or a hydroxyl (-OH) group (to provide a hydrophilic background) as shown in Figure S3. The alkyl thiol chains of the SAM strands were modeled as OPLS united atoms [39], while the -OH and ligand headgroups were parametrized based on Generalized Amber Force Field (GAFF) [40,41] parameters and AM1-BCC charges [42].

A harmonic potential of 1000 kcal/mol.A2 was applied to the sulfur atom and the seventh carbon from the sulfur to maintain the structure of the surface, as has been done previously [36–38]. The positions and orientations of the SAM strands correspond to an alkyl thiol SAM immobilized on a gold (1 1 1) surface [43]. The TIP3P [44] model was used to model water molecules, and chlorine counterions were used for electroneutrality. A box size of 10.978 nm x 10.368 nm x 10 nm was used resulting in surfaces with 528 SAM strands, of which 36, 88 and 132 were ligand strands for Prototypes 15, 6326–54, and 6611–9–1 SAMs respectively, to correspond to surface densities (0.3 ligands/nm2, 0.8 ligands/nm2 and 1.2 ligands/nm2) close to those on the resin. Ligand SAM strands were placed so that the pattern was not affected by the periodic boundary conditions at the edge of the box.

Each simulation was performed using GROMACS 2019.4 [45] in the NPT ensemble. The Parrinello-Rahman [46] barostat (semi-isotropic) and Nose-Hoover [47] thermostat were used to maintain a 1 bar pressure and 298 K temperature, respectively. Electrostatics were calculated using the particle-mesh Ewald [48] method with a grid spacing of 0.1 nm, a fourth order B-spline, and a direct sum tolerance of 10–5 (consistent with default parameters). The non-bonded cutoff was 0.9 nm. Bonds containing hydrogens were constrained using the LINCS [49] algorithm. Production runs for the MD were run for 20 ns (with a time-step of 2fs), saving frames every 2 ps.

3. Results and discussions

As described in the introduction, the effects of ligand chemistry and ligand geometry in multimodal anion exchange systems have been previously studied in our lab using homologous series of ligands [9,10,23]. The current work expands this analysis to include new classes of guanidine-based ligands, and to explore selectivity in these multimodal anion exchange systems. Further, we examine the efficacy of these resins when used in concert with a commercial multimodal cation exchange system to create orthogonally selective separation systems.

3.1. Structure of multimodal anion exchange (MMA) adsorbents

The structure of the multimodal anion exchange (MMA) ligands examined in this work are presented in Fig. 1. As can be seen, this included the commercial adsorbents Capto Adhere and Nuvia aPrime 4A along with three guanidine-based adsorbents (Prototypes 15, 6326–54 and 6611–9–1). In contrast to the commercial materials, the three guanidine class prototypes ligands were tethered to the matrix via the aromatic end of the ligand. While the ligand densities of the commercial adsorbents were approximately 100 µmol/ml, the prototypes varied in their ligand densities. Prototype resins 15 and 6326–54 had the same ligand structure with a single guanidine moiety and ligand densities of 53 and 90 µmol/ml, respectively. In contrast, Prototype 6611–9–1 possessed a bis-guanidine moiety at a ligand density of 133 µmol/ml.

3.2. Selectivity studies of model proteins at pH 7.0

The chromatographic behavior of a set of model acidic proteins on these MMA resins was first examined using linear gradient chromatography at pH 7 (representative chromatograms for BLA on the Nuvia aPrime 4A, Prototype 15 and Prototype 6611–9–1 are presented in SI Figure-1). The elution salt concentration at the first moment of the peaks is given in Fig. 2, arranged according to the elution order on Nuvia aPrime 4A. As can be seen, all proteins exhibited their lowest salt elution concentrations on this commercial resin. Protein elution on the other commercial MMA material, Capto adhere, closely followed the Nuvia aPrime 4A trend, albeit

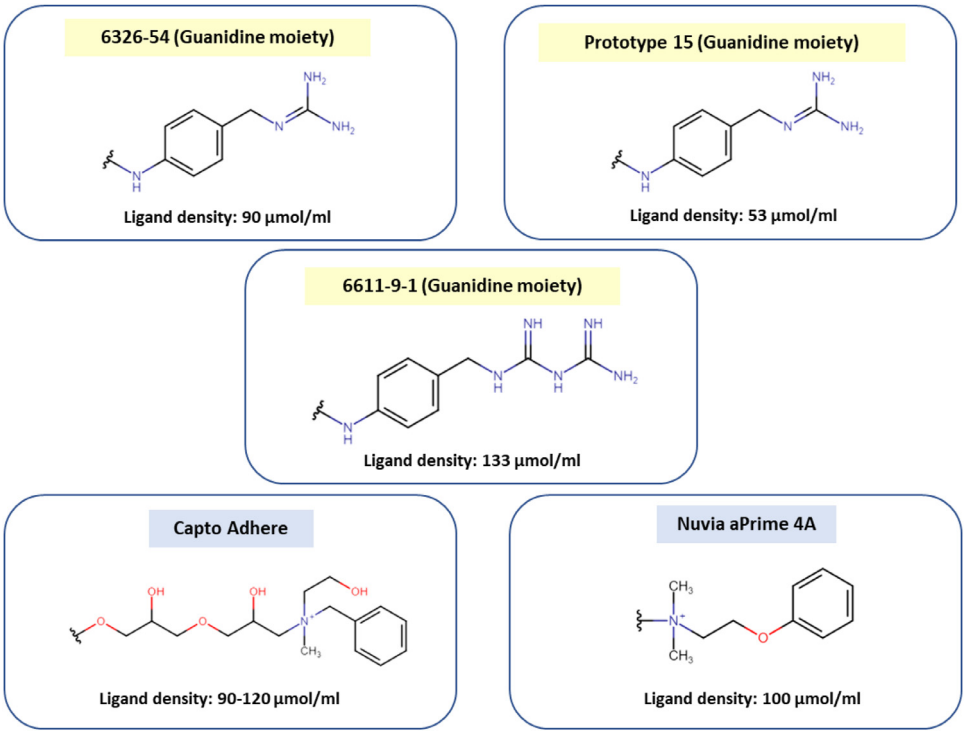

Fig. 1. Ligand structures and ligand densities of the multimodal anion exchange adsorbents used in this study.

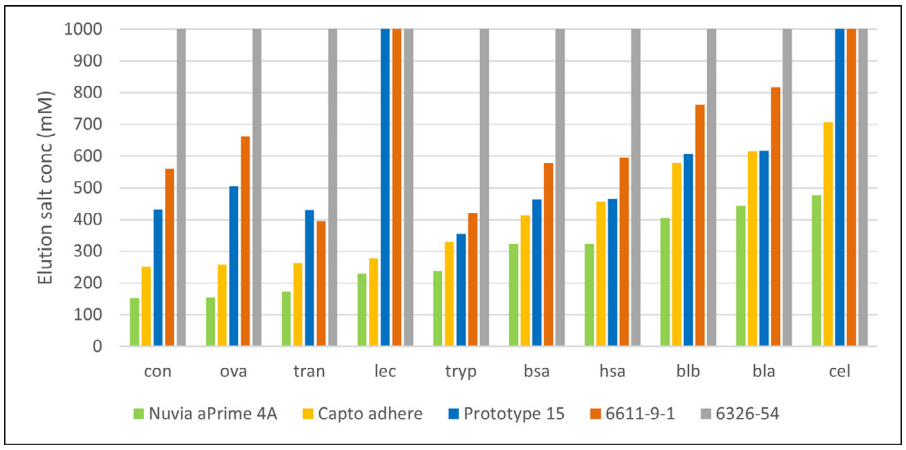

Fig. 2. Linear gradient chromatographic retention data of the model proteins at pH 7 on the multimodal anion exchange adsorbents.

with moderately higher elution salt concentrations. Interestingly, none of the model proteins were observed to elute from the high density, single guanidine Prototype 6326–54 resin. In sharp contrast, most of the model proteins eluted in the salt gradient on the lower ligand density material, Prototype 15, with the exceptions of lectin and cellulase. The results with the bis-guanidine Prototype 6611–9–1 material were quite different. Even at the high ligand density, the proteins eluted in the salt gradient, again with the exception of lectin and cellulase. From an operational point of view, it is interesting to note that both Prototypes 15 and 6611–9–1, exhibited higher elution salt concentrations for the early eluting proteins as compared to the commercial MMA resins. Further, for the more strongly bound proteins, while Prototype 15 had similar elution salt concentrations to the Capto adhere, Prototype 6611–9–1 had consistently higher elution salt concentrations and larger differences in the elution salt concentrations. The elution order of some of the proteins was also different in these systems. As can be seen in Fig. 2, while the elution salt for transferrin on Prototype 6611–9–1 was significantly lower than for ovalbumin, on the commercial materials these two proteins had very similar elution conditions. The elution trends observed with these guanidine-based prototypes were different than those observed in previous work from our lab [27]. Another important observation is regarding the peak shapes obtained during the gradient elution on these MMA adsorbents (SI Figure-1). The same model protein (BLA) showed varying peak widths on these MMA adsorbents which is indicative of the differing multimodal interactions between these adsorbents and protein. To illustrate this further, the protein elution data at pH 7 on these guanidine-based prototypes were examined using a QSAR model previously developed for an alternative set of multimodal anion exchange resins [27]. As can be seen in SI Figure-2, even though this previous model could predict a few data points from Prototype 15 within 100 mM elution salt, most of the elution data of the two guanidine prototypes were under-predicted, some up to 450 mM NaCl. This resulted in −1.08 and −2.60 R^2 scores for the single guanidine and bis-guanidine prototypes,

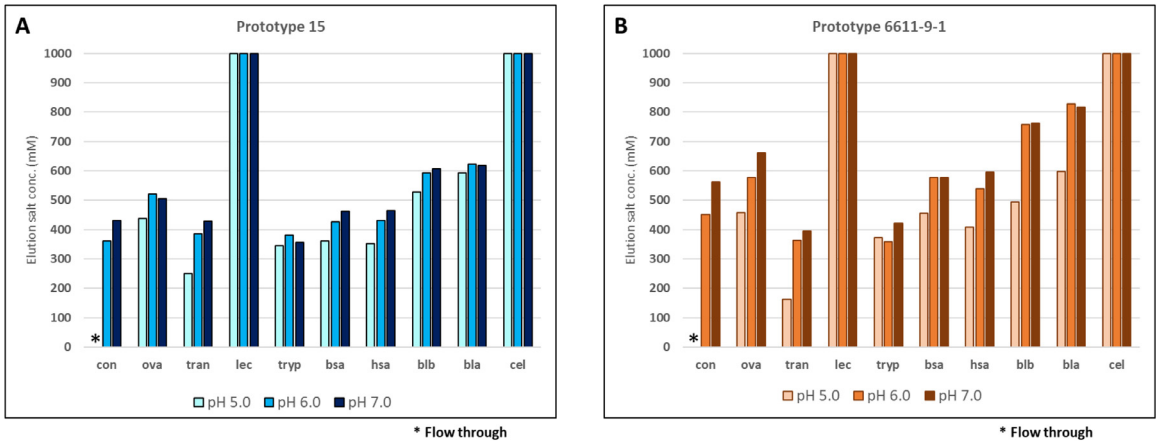

Fig. 3. Linear gradient chromatographic retention data of the model proteins at pH 5, 6 and 7 on (A) Prototype 15 and (B) Prototype 6611–9–1.

respectively. These results demonstrate that these two new guanidine prototypes are indeed different from the other MMA resins since their data is not in the applicability domain of the previously developed QSAR model. To further evaluate the selectivities that can be achieved with these new MMA prototypes, we evaluated the retention of this model protein set as a function of pH.

3.3. Comparison of pH-based selectivity in prototype 15 and prototype 6611–9–1

The impact of pH on the elution salt concentrations of the model proteins on the Prototypes are presented in Fig. 3. For the single guanidine Prototype 15, a similar selectivity pattern of the model proteins was seen at pH 5, 6, and 7 (Fig. 3a). While the retention decreased for some of the proteins at the lower pH, the differences were minimal except for the proteins conalbumin and transferrin which showed significant reductions in elution salt. In fact, conalbumin eluted in the flow-through at pH 5. It is interesting to note that these two proteins had the highest pIs of the model protein set with pIs of 6.77 and 6.83 for conalbumin and transferrin, respectively.

The results with Prototype 6611–9–1 are presented in Fig. 3b. The salt tolerance and higher elution salt concentrations observed at pH 7 with this resin were also seen at pH 6. While the presence of the two guanidine moieties in Prototype 6611–9–1 resulted in a general higher salt tolerance, the selectivity pattern for this resin was qualitatively similar to that seen for Prototype 15 at all pH conditions. However, the impact of pH on the relative retention results with Prototype 6611–9–1 was quite significant. In contrast to the results with Prototype 15, the elution behavior at pH 6 was reduced compared to pH 7 for five of the model proteins (conalbumin, ovalbumin, transferrin, trypsin inhibitor and HSA). At pH 5, the elution salt concentrations of these proteins were further reduced and an additional three proteins (BSA, BLB and BLA) exhibited a reduction in retention. These results are quite interesting in that they demonstrate that several of the more strongly retained proteins had a pH dependence in Prototype 6611–9–1 that was not achievable with the single guanidine ligand. Taken together, these results clearly demonstrate that Prototype 6611–9–1 not only has enhanced salt tolerance but also exhibits a strong pH dependence of protein retention. This unique behavior may offer some advantages for creating uniquely selective multimodal anion exchange separation processes.

Since unique selectivites can be achieved with the guanidine based resins, it was also of interest to generate a QSAR model for *in silico* prediction. As described in the methods section, partial least square (PLS) regression was employed to predict protein elution salt concentrations based on ten protein descriptors and one ligand descriptor selected from an initial pool of 576 features. As shown in Fig. 4, this PLS model was well suited for predicting the selectivity behavior of the two guanidine prototypes with overall training and test scores of 0.88 and 0.85, respectively. The model was shown to be stable with minimal overfitting as evaluated by y scrambling [50] and the RMSD of the training and testing sets were 56 and 77 mM, respectively, again indicating good overall performance. While the model was quite accurate in the range of 300 to 700 mM NaCl where there was a lot of data, the predictions at higher salts were less precise. The ability to predict protein retention in these guanidine-based MMA adsorbents at various pH may be a useful tool to facilitate process development. Interestingly, most of the protein descriptors included in this model related to protein surface charge characteristics, indicating that electrostatic interactions played an important role in determining the elution behavior. Further, the only ligand descriptor selected was 'the number of nitrogen atoms in the ligand' which likely served as a surrogate for distinguishing the charge properties between the single and double guanidine prototypes. To better understand the mechanism behind these different selectivity trends, molecular dynamics simulations of a ligand coated surface were carried out which will be discussed below.

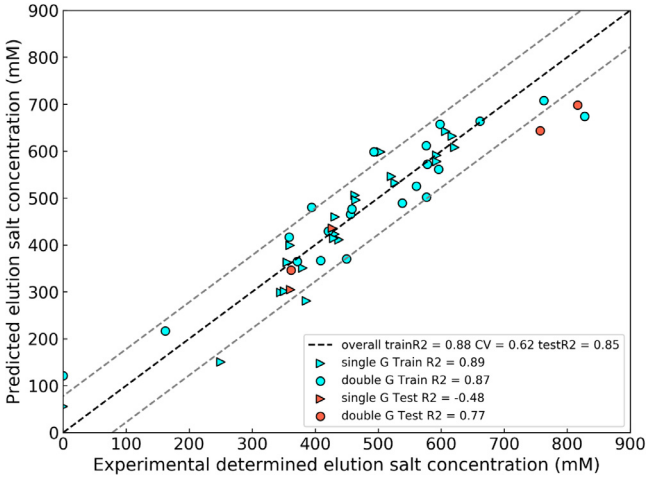

Fig. 4. QSAR model predictions for Prototype 15 (triangle) and Prototype 6611–9–1 (circle) at multiple pH. Training data are in turquoise and testing data are in red. The gray dotted lines represent the RMSD values of the test set. (For interpretation of the references to colour in this figure legend, the reader is referred to the web version of this article.)

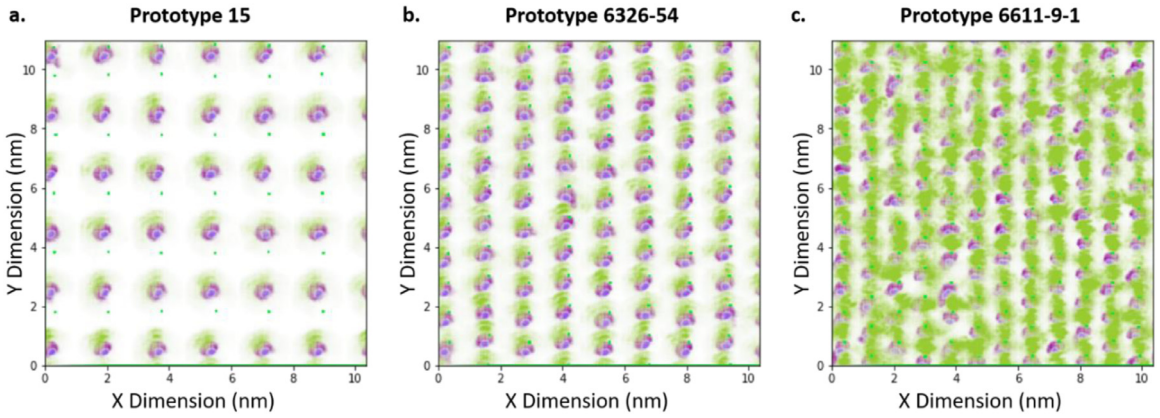

Fig. 5. Density distributions for ligands immobilized on SAM surfaces at densities close to their respective resin density. The results were obtained using a single 20 ns trajectory. The atom density scale ranges from 0 (white) to 2 atoms/nm^2 (relevant color). Colors: purple, phenyl ring; dull green, guanidine group; blue, ligand base nitrogen and bright green, SAM sulfur grid. (For interpretation of the references to colour in this figure legend, the reader is referred to the web version of this article.)

3.4. Molecular dynamics studies with ligand immobilized sam surfaces

To gain further insight into the molecular behavior of these prototype ligands, MD simulations of ligand immobilized SAM surfaces were performed in water. Ligands were placed uniformly on the SAM surface, with the number of immobilization sites chosen to correspond to a surface density similar to that on the resin material. Ligand conformation with respect to the surface was characterized by calculating the density distributions of these chemical moieties in the *x-y* plane of the surface. In addition, ligand conformation with respect to the surface normal (*z*-dimension) was also characterized using heavy atom number density distributions for individual chemical moieties on the ligand. These measures have been used previously by our group to characterize ligand clusters in MMC systems [37].

Fig. 5 show the density distributions (averaged over the entire trajectory) associated with the individual moieties; phenyl rings (purple), guanidine or bis-guanidine groups (dull green) and ligand base nitrogen (blue); on the guanidine based ligands. The sulfur atom density (bright green) illustrates the grid on which the SAM ligand strands are placed. For the single guanidine low density system (Prototypes 15, Fig. 5a), the phenyl ring (purple) can be seen to sample all positions around the base nitrogen (blue), indicating that the ligand is free to rotate around the point of immobilization. In addition, the guanidine group displays a preference for one direction due to the tilted SAM surface. At this lower ligand density, the ligands are sufficiently spaced such that both phenyl and guanidine moieties would be available for interactions with a protein. Even when the density is increased for the single guanidine resin (Prototype 6326–54, Fig. 5b), the phenyl groups (purple) remain solvent accessible. It is also informative to examine the heavy atom density distributions of the single guanidine ligand surfaces (Figure S4(a,c) along with representative snapshots of the ligand SAM surface (Figure S4 b and d). The location of the phenyl group peaks indicates that the ligands rarely flatten out, but do adopt either a slightly bent or a completely outstretched conformation. In addition, the snapshots illustrate the solvent exposure of the phenyl moieties. These preferences of the single guanidine ligands imply that there is a high likelihood of hydrophobic (driven by the phenyl groups) as well as electrostatic (driven by the guanidine groups) interactions with the protein.

Fig. 5c shows moiety density distributions for the bis-guanidine ligand surface (Prototype 6611–9–1) with the corresponding heavy atom densities and representative snapshots given in Figure S4(e,f). As can be seen in Fig. 5c, this surface presents a relatively uniform surface pattern, with a layer of the charged bis-guanidine group on top of the less accessible phenyl group layer. This is due to both the higher ligand density as well as the predominance of the outstretched ligand conformation due to charge-charge repulsion. The relative inaccessibility of the phenyl group combined with the solvent exposure of the bis-guanidine groups indicates that interactions between proteins and this ligand surface may be more electrostatically driven than with the single guanidine systems examined. These subtle differences in ligand conformational preferences and relative solvent exposure of the phenyl moieties help to explain the difference in protein recoveries observed in the high density single and bis-guanidine resin systems.

3.5. Orthogonality studies with bis-guanidine prototype

As described in the introduction, we have developed a formalism for quantifying the separability and orthogonality of resin combinations for separating proteins [33]. As discussed above, Nuvia aPrime 4A and Prototype 6611–9–1 had significant differences in their selectivities as well as the relative contributions of hydrophobicity to protein retention. Thus, it was of interest to examine their ability to work in conjunction with a commercial MMC resin (Nuvia cPrime) to create enhanced selectivity. As indicated in the experimental section, for this analysis a protein set was employed that included both acidic and basic model proteins with varying levels of hydrophobicity.

Fig. 6 presents the results with both MMA resins at pH 7 and the Nuvia cPrime resin at pH 5. It is interesting to note that even basic hydrophobic proteins exhibited different selectivity on MMA Prototype 6611–9–1 as compared to the commercial Nuvia aPrime 4A resin. Importantly, the bis-guanidine resin (Prototype 6611–9–1) had higher separability for this particular protein set (0.51) as compared to the less hydrophobic Nuvia aPrime 4A MMA material (0.25). Further, the Prototype 6611–9–1 was seen to be more orthogonal when used in conjunction with Nuvia cPrime as compared to the Nuvia aPrime 4A chromatographic material, again for this protein set. This can be seen both in the distribution of the retention data on the two figures as well as in the higher pair separability factor (0.73) and pair enhancement factor (0.42) obtained with the Prototype 6611–9–1 – Nuvia cPrime combination. While the increased hydrophobicity and retention of some of the proteins on Prototype 6611–9–1 helped to make it more orthogonal, three of the proteins did not elute under these conditions and would likely require a shift in pH if they were the desired product.

These results are encouraging in that they demonstrate that not only does Prototype 6611–9–1 (bis-guanidine adsorbent) have

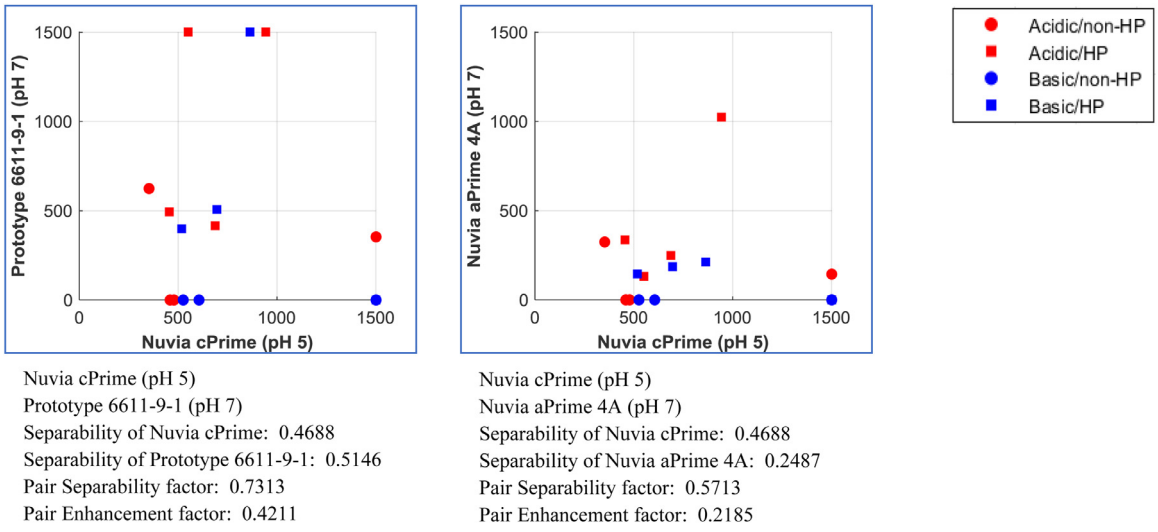

Fig. 6. Orthogonality plots of Nuvia cPrime at pH 5 with Prototype 6611–9–1 and Nuvia aPrime 4A at pH 7.

many useful properties such as salt tolerance, facile elution and unique selectivity (particularly for hydrophobic proteins); but that when used in conjunction with Nuvia cPrime, there may be an opportunity to address a range of separation challenges in downstream bioprocessing.

4. Conclusions

This work studied the chromatographic behavior of a new class of guanidine based multimodal anion exchange resins. The results indicated that higher selectivities were achieved with a bis-guanidine ligand-based resin as compared to a single guanidine ligand resin at low ligand densities, particularly for more retained proteins. Interestingly, the significant recovery issues observed with a high density single guanidine ligand resin were not observed for the bis-guanidine ligand based resin. An evaluation of both the separability of the top performing bis-guanidine resin as well as its orthogonality to the commercial multimodal cation exchange Nuvia cPrime resin was also carried out. Importantly, the results indicated that the bis-guanidine prototype exhibited both high separability and orthogonality for the protein set evaluated. The enhanced selectivity, orthogonality and protein recovery of this new multimodal anion exchange ligand may offer interesting opportunities for bioprocessing applications.

Future work will examine the underlying physics for the selectivity and pH dependence of the bis-guanidine resin system using a variety of *in silico* and biophysical techniques. This will include molecular dynamic simulations and dewetting calculations for these ligand-coated surfaces to better understand protein binding and desolvation effects in these systems. This work will also examine the impact of ligand density on the separability, orthogonality and protein recoveries in these systems. Finally, the utility of this new MMA resin will be evaluated for a variety of flow-through and bind elute bioprocessing applications.

Declaration of Competing Interest

The authors declare that they have no known competing financial interests or personal relationships that could have appeared to influence the work reported in this paper.

The authors declare the following financial interests/personal relationships which may be considered as potential competing interests:

CRediT authorship contribution statement

Sushmita Koley: Conceptualization, Data curation, Formal analysis, Investigation, Methodology, Project administration, Resources, Software, Supervision, Validation, Visualization, Writing – original draft, Writing – review & editing. **Scott H. Altern:** Data curation, Formal analysis, Methodology, Software, Writing – review & editing. **Mayank Vats:** Data curation, Formal analysis, Methodology, Software, Writing – review & editing. **Xuan Han:** Data curation, Formal analysis, Methodology, Software, Writing – review & editing. **Dongyoun Jang:** Investigation, Validation. **Mark A. Snyder:** Conceptualization, Resources. **Chris Belisle:** Conceptualization, Resources. **Steven M. Cramer:** Conceptualization, Supervision, Writing – review & editing, Funding acquisition, Project administration.

Acknowledgements

This study was supported by Bio-Rad laboratories (Hercules, CA, 94547, USA) and the National Science Foundation (Grant number CBET 1704745).

Supplementary materials

Supplementary material associated with this article can be found, in the online version, at doi:10.1016/j.chroma.2021.462398.

References

[1] S.M. Cramer, M.A. Holstein, Downstream bioprocessing: recent advances and future promise, Curr. Opin. Chem. Eng. 1 (2011) 27–37.
[2] I.F. Pinto, M.R. Aires-Barros, A.M. Azevedo, Multimodal chromatography: debottlenecking the downstream processing of monoclonal antibodies, Pharm. Bioprocess. 3 (2015) 263–279.
[3] K. Kallberg, H.O. Johansson, L. Bulow, Multimodal chromatography: an efficient tool in downstream processing of proteins, Biotechnol. J. 7 (2012) 1485–1495.
[4] G. Zhao, X. Dong, Y. Sun, Ligands for mixed-mode protein chromatography: principles, characteristics and design, J. Biotechnol. 144 (2009) 3–11.
[5] V. Halan, S. Maity, R. Bhambure, A.S. Rathore, Multimodal chromatography for purification of biotherapeutics – a review, Curr. Protein Pept. Sci. 20 (2018) 4–13.
[6] L.E. Crowell, A.E. Lu, K.R. Love, A. Stockdale, S.M. Timmick, D. Wu, Y.A. Wang, W. Doherty, A. Bonnyman, N. Vecchiarello, C. Goodwine, L. Bradbury, J.R. Brady, J.J. Clark, N.A. Colant, A. Cvetkovic, N.C. Dalvie, D. Liu, Y. Liu, C.A. Mascarenhas, C.B. Matthews, N.J. Mozdzierz, K.A. Shah, S.L. Wu, W.S. Hancock, R.D. Braatz, S.M. Cramer, J.C. Love, On-demand manufacturing of clinical-quality biopharmaceuticals, Nat. Biotechnol. 36 (2018) 988.
[7] Y. Li, Y. Sun, Poly(4-vinylpyridine): a polymeric ligand for mixed-mode protein chromatography, J. Chromatogr. A 1373 (2014) 97–105.

[8] D.S. Chai, Y. Sun, X.N. Wang, Q.H. Shi, Improved purification of immunoglobulin G from plasma by mixed-mode chromatography, J. Sep. Sci. 37 (2014) 3461–3472.
[9] J. Woo, S. Parimal, M.R. Brown, R. Heden, S.M. Cramer, The effect of geometrical presentation of multimodal cation-exchange ligands on selective recognition of hydrophobic regions on protein surfaces, J. Chromatogr. A 1412 (2015) 33–42.
[10] J.A. Woo, H. Chen, M.A. Snyder, Y. Chai, R.G. Frost, S.M. Cramer, Defining the property space for chromatographic ligands from a homologous series of mixed-mode ligands, J. Chromatogr. A 1407 (2015) 58–68.
[11] D. Gao, D.Q. Lin, S.J. Yao, Mechanistic analysis on the effects of salt concentration and pH on protein adsorption onto a mixed-mode adsorbent with cation ligand, J. Chromatogr. B Anal. Technol. Biomed. Life Sci. 859 (2007) 16–23.
[12] B.K. Nfor, M. Noverraz, S. Chilamkurthi, P.D.E.M. Verhaert, L.A.M. van der Wielen, M. Ottens, High-throughput isotherm determination and thermodynamic modeling of protein adsorption on mixed mode adsorbents, J. Chromatogr. A 1217 (2010) 6829–6850.
[13] M. Zhu, G. Carta, Protein adsorption equilibrium and kinetics in multimodal cation exchange resins, Adsorption 22 (2016) 165–179.
[14] J.P. Welsh, H. Bao, K. Barlow, J.M. Pollard, E. Brekkan, K.M. Lacki, T.O. Linden, D.J. Roush, High-throughput techniques to evaluate the effect of ligand density for impurity separations with multimodal cation exchange resins, Eng. Life Sci. 16 (2016) 160–168.
[15] Y. Wang, Q. Chen, M. Xian, R. Nian, F. Xu, Application Of Enhanced Electronegative Multimodal Chromatography As The Primary Capture Step For Immunoglobulin G Purification, 8, AMB Express, 2018.
[16] P. Gagnon, C.W. Cheung, E.J. Lepin, A.M. Wu, M.A. Sherman, A.A. Raubitschek, P.J. Yazaki, Minibodies and multimodal chromatography methods: a convergence of challenge and opportunity, Bioprocess Int 8 (2) (2010) 26–35.
[17] R. Bhambure, D. Gupta, A.S. Rathore, A novel multimodal chromatography based single step purification process for efficient manufacturing of an E. coli based biotherapeutic protein product, J. Chromatogr. A. 1314 (2013) 188–198.
[18] G. Joucla, C.Le Sénéchal, M. Bégorre, B. Garbay, X. Santarelli, C. Cabanne, Cation exchange versus multimodal cation exchange resins for antibody capture from CHO supernatants: identification of contaminating host cell proteins by mass spectrometry, J. Chromatogr. B 942–943 (2013) 126–133.
[19] X. Fan, Y. Zhou, J. Yu, F. Li, Q. Chen, H. Song, D. Feng, W. Liu, R. Nian, M. Xian, Non-affinity purification of a nanobody by void-exclusion anion exchange chromatography and multimodal weak cation exchange chromatography, Sep. Purif. Technol. 225 (2019) 88–96.
[20] K.A. Kaleas, M. Tripodi, S. Revelli, V. Sharma, S.A. Pizarro, Evaluation of a multimodal resin for selective capture of CHO-derived monoclonal antibodies directly from harvested cell culture fluid, J. Chromatogr. B Anal. Technol. Biomed. Life Sci. 969 (2014) 256–263.
[21] L. Zhang, S. Parasnavis, Z. Li, J. Chen, S. Cramer, Mechanistic modeling based process development for monoclonal antibody monomer-aggregate separations in multimodal cation exchange chromatography, J. Chromatogr. A (2019).
[22] L.S. Wolfe, C.P. Barringer, S.S. Mostafa, A.A. Shukla, Multimodal chromatography: characterization of protein binding and selectivity enhancement through mobile phase modulators, J. Chromatogr. A 1340 (2014) 151–156.
[23] R.A. Chmielowski, S. Meissner, D. Roush, T.O. Linden, E. Glowacki, J. Konietzko, J. Nti-gyabaah, Resolution of heterogeneous charged antibody aggregates via multimodal chromatography: a comparison to conventional approaches, AIChE (2014) 636–645.
[24] J. Chen, J. Tetrault, Y. Zhang, A. Wasserman, G. Conley, M. Dileo, E. Haimes, A.E. Nixon, A. Ley, The distinctive separation attributes of mixed-mode resins and their application in monoclonal antibody downstream purification process, 1217 (2010) 216–224.
[25] E.O. Connor, M. Aspelund, F. Bartnik, M. Berge, K. Coughlin, M. Kambarami, D. Spencer, H. Yan, W. Wang, Monoclonal antibody fragment removal mediated by mixed mode resins, J. Chromatogr. A 1499 (2017) 65–77.
[26] B. Johansson, M. Belew, S. Eriksson, G. Glad, O. Lind, J. Maloisel, N. Norrman, Preparation and characterization of prototypes for multi-modal separation media aimed for capture of negatively charged biomolecules at high salt conditions, J. Chromatogr. A 1016 (2003) 21–33.
[27] J. Robinson, M.A. Snyder, C. Belisle, J. Ii Liao, H. Chen, X. He, Y. Xu, S.M. Cramer, Investigating the impact of aromatic ring substitutions on selectivity for a multimodal anion exchange prototype library, J. Chromatogr. A 1569 (2018) 101–109.
[28] J. Pezzini, C. Cabanne, J.W. Dupuy, R. Gantier, X. Santarelli, A study on the nature of interactions of mixed-mode ligands HEA and PPA HyperCel using phenylglyoxal modified lysozyme, J. Chromatogr. B Anal. Technol. Biomed. Life Sci. 960 (2014) 209–213.
[29] B.L. Johansson, M. Belew, S. Eriksson, G. Glad, O. Lind, J.L. Maloisel, N. Norrman, Preparation and characterization of prototypes for multi-modal separation aimed for capture of positively charged biomolecules at high-salt conditions, J. Chromatogr. A 1016 (2003) 35–49.
[30] V. Brenac Brochier, A. Schapman, P. Santambien, L. Britsch, Fast purification process optimization using mixed-mode chromatography sorbents in pre–packed mini-columns, J. Chromatogr. A 1177 (2008) 226–233.
[31] E. Boschetti, Antibody separation by hydrophobic charge induction chromatography, Trends Biotechnol. 20 (2002) 333–337.
[32] N. Vecchiarello, S.M. Timmick, C. Goodwine, L.E. Crowell, K.R. Love, J.C. Love, S.M. Cramer, A combined screening and in silico strategy for the rapid design of integrated downstream processes for process and product-related impurity removal, Biotechnol Bioeng. 116 (2019) 2178–2190.
[33] C.L. Bilodeau, N.A. Vecchiarello, S. Altern, S.M. Cramer, Quantifying orthogonality and separability: a Method for optimizing resin selection and design, J. Chromatogr. A (2020) 461429.
[34] D. Shukla, B.L. Trout, Interaction of arginine with proteins and the mechanism by which it inhibits aggregation, J. Phys. Chem. B 114 (2010) 13426–13438.
[35] D. Shukla, L. Zamolo, C. Cavallotti, B.L. Trout, Understanding the role of arginine as an eluent in affinity chromatography via molecular computations, J. Phys. Chem. B 115 (2011) 2645–2654.
[36] S. Banerjee, S. Parimal, S.M. Cramer, A molecular modeling based method to predict elution behavior and binding patches of proteins in multimodal chromatography, J. Chromatogr. A 1511 (2017) 45–58.
[37] C.L. Bilodeau, E.Y. Lau, D. Roush, S. Garde, S.M. Cramer, Formation of ligand clusters on multimodal chromatographic surfaces, Langmuir 35 (2019) 16770–16779.
[38] N. Shenogina, R. Godawat, P. Keblinski, S. Garde, How wetting and adhesion affect thermal conductance of a range of hydrophobic to hydrophilic aqueous interfaces, Phys. Rev. Lett. 102 (2009) 1–4.
[39] M. Mondello, G.S. Grest, E.B. Webb, P. Peczak, Dynamics of n-alkanes: comparison to Rouse model, J. Chem. Phys. 109 (1998) 798–805.
[40] C.I. Bayly, K.M. Merz, D.M. Ferguson, W.D. Cornell, T. Fox, J.W. Caldwell, P.A. Kollman, P. Cieplak, I.R. Gould, D.C. Spellmeyer, A second generation force field for the simulation of proteins, nucleic acids, and organic molecules, J. Am. Chem. Soc. 117 (1995) 5179–5197.
[41] J. Wang, R.M. Wolf, J.W. Caldwell, P.A. Kollman, D.A. Case, J. Comput. Chem. 56531 (2004) 1157–1174.
[42] A. Jakalian, D.B. Jack, C.I. Bayly, Fast, efficient generation of high-quality atomic charges. AM1-BCC model: II. Parameterization and validation, J. Comput. Chem. 23 (2002) 1623–1641.
[43] H. Kind, J.M. Bonard, C. Emmenegger, L.O. Nilsson, K. Hernadi, E. Maillard-Schaller, L. Schlapbach, L. Forró, K. Kern, Patterned films of nanotubes using microcontact printing of catalysts, 1999.
[44] P. Mark, L. Nilsson, Structure and dynamics of the TIP3P, SPC, and SPC/E water models at 298K, J. Phys. Chem. A. 105 (2001) 9954–9960.
[45] M.J. Abraham, T. Murtola, R. Schulz, S. Páll, J.C. Smith, B. Hess, E. Lindah, Gromacs: high performance molecular simulations through multi-level parallelism from laptops to supercomputers, SoftwareX 1–2 (2015) 19–25.
[46] M. Parrinello, A. Rahman, Crystal structure and pair potentials: a molecular–dynamics study, Phys. Rev. Lett. 45 (1980) 1196–1199.
[47] D.J. Evans, B.L. Holian, The Nose-Hoover thermostat, J. Chem. Phys. 83 (1985) 4069–4074.
[48] T. Darden, D. York, L. Pedersen, Particle mesh ewald: an N-log(N) method for ewald sums in large systems, J. Chem. Phys. 98 (1993) 10089–10092.
[49] B. Hess, H. Bekker, H.J.C. Berendsen, J.G.E.M. Fraaije, LINCS: a Linear Constraint Solver for molecular simulations, J. Comput. Chem. 18 (1997) 1463–1472.
[50] R. Veerasamy, H. Rajak, A. Jain, S. Sivadasan, C.P. Varghese, R.K. Agrawal, Validation of QSAR models - strategies and importance, Int. J. Drug Des. Disocovery. 2 (2011) 511–519.